X-ray spectrum of a laser-produced iron plasma*

L. F. Chase, W. C. Jordan, and J. D. Perez
Lockheed Palo Alto Research Laboratory, 3251 Hanover Street, Palo Alto, California 94304

R. R. Johnston
Science Applications, Inc., 2680 Hanover Street, Palo Alto, California 94304

(Received 29 September 1975; revised manuscript received 12 January 1976)

We present the analysis of the x-ray spectrum between 9.5 and 17.0 Å of a laser-produced iron plasma. Wavelengths and relative intensities for 96 lines are measured. For the strongest part of the spectrum, above 13 Å, almost all of the observed lines are identified as radiation from Fe^{XVII}, Fe^{XVIII}, and Fe^{XIX} ions. Measurements were made with a curved-crystal spectrograph. Calculations were full intermediate coupling, Hartree-Fock with relativistic corrections. Coulomb-approximation oscillator strengths were used to help in the line identification.

I. INTRODUCTION

The x-ray spectrum of an iron plasma has been studied in the solar corona,[1-7] in iron-spark and plasma focus, in laboratory plasmas,[8-14] and in laser-produced plasmas.[1,15] The accurate measurement and identication of spectral lines is important as a diagnostic tool for both astrophysical and laboratory plasmas.

We present the measurement and analysis of the x-ray spectrum between 9.5 and 17.0 Å (approximately 1300–700 eV) of a laser-produced iron plasma. The plasma was created by a 100-J, 2-nsec, 1.06-μm laser pulse focused to an area of about 200 μm diameter on a high-purity iron target (approximately 10^{14} W/cm^2).[16] Almost all of the intense lines observed between 13 and 17 Å are assigned to transitions arising in Fe^{XVII} through Fe^{XIX}. These assignments represent a number of new identifications, as well as assignment of J values to many transitions previously only partially identified. For the shorter wavelengths, the intensity of the observed lines is generally lower and, in addition, the number of closely overlapping, calculated transitions is high. Thus positive identification of these lines is impossible in most cases. Theoretical values for the wavelengths in Fe^{XVII}, Fe^{XVIII}, and Fe^{XIX} were obtained by performing Hartree-Fock[17] intermediate coupling calculations with relativistic corrections. The calculated values agreed with the data to within 0.25%.

The measured wavelengths and intensities of the observed lines are presented. Good agreement is obtained between the wavelengths of the lines measured in the present work and various previous observations in the region of overlapping measurements.[5,9,11,13,14] The agreement are both gratifying and interesting since, in general, the nature of both the source and the instrumentation were quite different. The experimental arrangement is described in Sec. II.

The calculation of the wavelengths and oscillator strengths are outlined in Sec. III. Several previous calculations of the wavelengths[7,10,12,18-20] have been similar in spirit to ours but, while including intermediate coupling to some extent, have LS quantum numbers to identify the transitions. We find such strong intermediate coupling that it is appropriate to specify only the single-electron transition and the initial and final total angular momentum. The breakdown of LS coupling in Fe^{XVIII} lines has been observed previously in Ref. 14.

In order to aid in the complete identification of the lines, we used oscillator strengths from the Coulomb approximation.[21] Comparison with configuration-mixing calculation[22] of Fe^{XVII} oscillator strengths shows the Coulomb-approximation values to be accurate to a factor of 2 or 3.

II. EXPERIMENTAL APPARATUS

The experimental data were obtained with a multichannel curved-crystal spectrograph designed especially for pulsed source use. The plasma source was produced at the Laser Facility of the Battelle Memorial Institute. Incident radiation of 1.06 μm was generated by a Q-switched neodymium-glass laser system and focused on the surface of a high-purity iron target. The time duration of the main pulse was about 1.5 nsec, and the incident energy was in the range 80–100 J for most of the irradiations. The spectrograph observed the x-rays emitted at 90° to the incident laser beam, with the targets oriented at 45° to the beam. Spec-

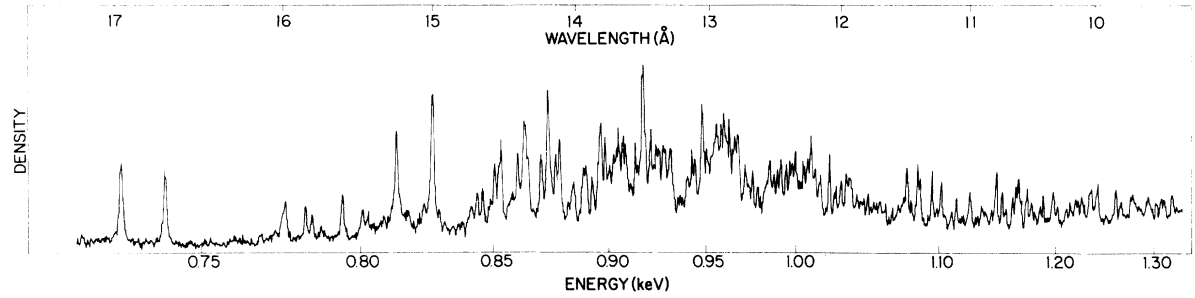

FIG. 1. Densitometer tracing of an iron-plasma spectrogram.

tra were recorded from several elements, but only the iron data are presented here. A typical densitometer tracing of an iron spectrogram is shown in Fig. 1.

In the operational mode used in these experiments three KAP (potassium acid phthlate) crystals were mounted in the spectrograph, as shown schematically in Fig. 2. The radiation is incident upon the convex side of the crystals in a three-beam pattern defined by the source and three aperture slits at the entrance of the spectrograph. Each crystal was bent along a 20° arc with a radius of 12.7 cm. Thus each crystal covered an angular range of Bragg scattering somewhat larger than 40° (twice the sum of the crystal arc and divergence angle of the incident radiation). The orientation angle (α in Fig. 2) could be adjusted independently for each crystal. Typically this was set at 10° for one crystal, 20° for the second, and 30° for the third. The dispersed radiation from each crystal was incident upon a common x-ray film (Kodak No-Screen) supported on a cylindrical frame whose axis was coincident with the axis of rotation of the crystals. Reference position marks were imprinted on the film at four lateral positions and at each 10° interval along the film by means of a light probe inserted through holes in the frame. These index marks provided a means of monitoring for dimensional changes in the film and allowed precise comparison of different films. The film holders were mounted in the spectrograph on a carriage that could be translated laterally with the spectrograph evacuated. Thus several spectrograms could be recorded from each crystal on a single film; the exact number depended upon several geometric factors, including the spacing desired between adjacent spectrograms. In a typical situation, three or four spectrograms were easily recorded with no overlap. To prevent "crosstalk" among the three crystals, baffles were used that, in effect, divide the spectrograph into three compartments.

The fundamental Bragg reflection condition corrected for refraction determines the true 2θ angle of scattering for a given incident energy. The position of a spectral line relative to the angular index marks imprinted on a film yields directly a quantity which may be defined as the apparent scattering angle ($2\theta_A$). The relation between $2\theta_A$ and 2θ is a geometrical calculation involving the source distance, the radius of the crystal, the angular orientation of the crystal, the lateral displacement (l in Fig. 2) of the crystal, and the radius of the film. Line-position data are recorded as distance from one or more of the reference index marks located at 10° intervals along the film. This information, together with the geometrical parameters, was fed into a simple computer program that calculated the true reflection angle and from this the observed energy, taking account

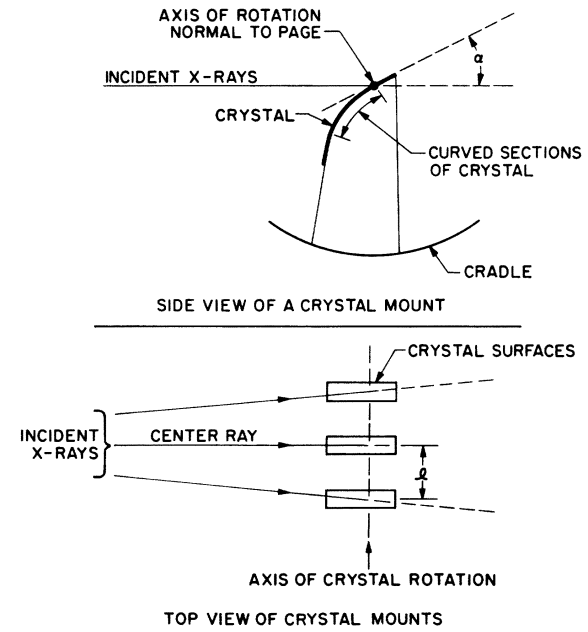

FIG. 2. Schematic presentation of the crystal and cradle orientations.

of the reflection order and the refraction effect at the crystal. Position-energy calibration data have been obtained using line radiation produced by a low-energy x-ray generator using an aluminum anode. In addition to the characteristic K radiation of aluminum, copper K and L, tungsten L and M, and silicon K radiation is emitted because of the natural buildup of these contaminants on the anode surface. A discontinuity in reflection of the continuum radiation at the K absorption edge of potassium in the KAP crystal also provides a data point. Although the Cu L_α radiation (929.7 eV) is the lowest energy, higher-order reflections extend the range of calibration. For example, the tenth-order Cu $K\alpha_1$ line and the second-order Al $K\alpha$ line are at positions equivalent to 804.8 and 743.3 eV, respectively.

For the energy region encompassing the iron-plasma data, five lines have been chosen as primary calibration points. These are Cu $K\alpha_1$ (sixth, seventh, and tenth order), Cu $L\alpha$ (first order), and Al $K\alpha$ (second order) at the transition-energy values listed by Bearden.[23] The energy values observed with various crystal orientations and lateral positions are in agreement with the true value, with an average deviation of about 0.02%, which is consistent with the uncertainty in the measurement of the line positions on the film. These data establish the accuracy of the transitions energies observed for the iron-plasma radiations on a relative basis. The absolute values may not be determined as accurately because of some uncertainty in the alignment of the apparatus with the laser target. However comparison with previous high-resolution measurements[5,14] shows no differences greater than 0.02 Å.

Calibration data have also been obtained to determine the sensitivity of three components: the transmission of the entrance window (0.3-μm Parylene-N with 0.2 μm of aluminum evaporated on each side), the reflectivity of the crystal, and the response of the x-ray emulsion. These were separately calibrated using fluorescent radiation of various energies. When combined, these data yield the relative sensitivity function shown in Fig. 3. The two discontinuities are due to the onset of aluminum K absorption in the window and potassium K absorption in the crystal.

III. LINE IDENTIFICATION

The objective of our theoretical study is the spectral identification of the principal iron lines observed. Toward this end we proceeded as in previous studies of high-temperature air opacity.[24,25]

For each charge state of the ion a complete set of L-S states is defined, and for each such state a numerical Hartree-Fock calculation is performed—with relativistic corrections. An intermediate-coupling calculation is then carried out, based on the Hartree-Fock results, and our final results for energy levels are obtained. Finally, application of electric dipole selection rules to the resulting intermediate-coupled states determined the spectra. The results we present here are for five to ten electrons bound to an iron nucleus ($Z = 26$).

The previous identifications[1-15] of x-ray lines in iron between 13 and 17 Å show that the strongest lines come from Fe^{XVII}, Fe^{XVIII}, and Fe^{XIX}; i.e., lines isoelectronic with Ne^{I}, F^{I}, and O^{I}, respectively. We used previous identifications and the calculated oscillator strengths as a guide in selecting the observed transitions from among the thousands in the intermediate-coupling calculation. The line identifications are listed in Table I along with the observed lines and their measured intensities.

The lines at shorter wavelengths generally had lower intensities. The measured wavelengths and intensities of the prominent lines are shown in Table II. The calculations for $Fe^{XVII\text{-}XIX}$ show a high density of closely spaced lines, making identification difficult. As noted in Table II, some of these lines may be identifiable as originating from more highly charged ionic states. A detailed model

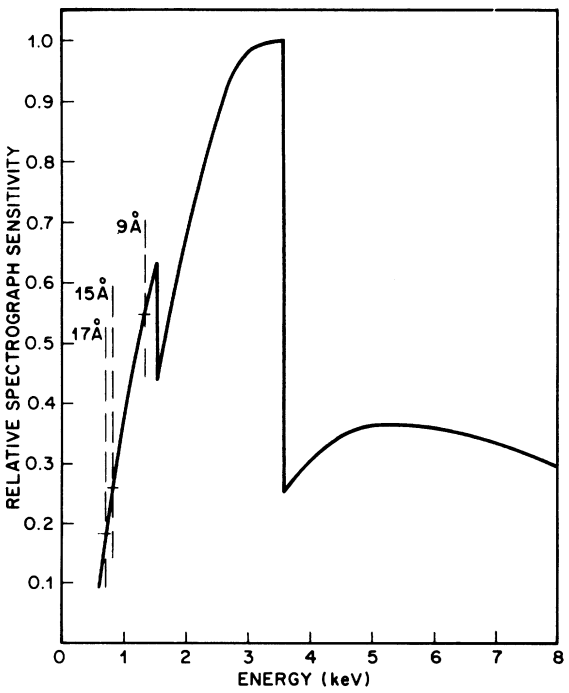

FIG. 3. Relative sensitivity of the spectrograph vs energy of the radiation.

TABLE I. Prominent observed lines between 13 and 17 Å compared to calculated wavelengths. The measured intensities are normalized so that the strongest line at 15.00 Å has intensity equal to unity.

I	λ (Å)	λ_{calc} (Å)	Charge state	$n'l' \rightarrow nl$	$J' \rightarrow J$	f_{calc}	Footnotes
0.51	17.04	17.06	XVII	$3s \rightarrow 2p$	$1 \rightarrow 0$	0.06	Ref. 8
0.48	16.76	16.79	XVII	$3s \rightarrow 2p$	$1 \rightarrow 0$	0.04	Ref. 8
0.29	16.00	16.01	XVIII	$3s \rightarrow 2p$	$\frac{3}{2} \rightarrow \frac{3}{2}$	0.01	a, Ref. 1
0.23	15.86	15.88	XVIII	$3s \rightarrow 2p$	$\frac{1}{2} \rightarrow \frac{3}{2}$	0.01	Ref. 1
0.13	15.82	15.84	XVIII	$3s \rightarrow 2p$	$\frac{3}{2} \rightarrow \frac{5}{2}$	0.02	Ref. 14
0.25	15.61	15.61	XVIII	$3s \rightarrow 2p$	$\frac{5}{2} \rightarrow \frac{3}{2}$	0.03	Ref. 1
		15.61	XVIII	$3s \rightarrow 2p$	$\frac{3}{2} \rightarrow \frac{3}{2}$	0.02	
0.13	15.48						
0.13	15.44	15.45	XVII	$3d \rightarrow 2p$	$1 \rightarrow 0$	0.01	Ref. 8
0.72	15.25	15.27	XVII	$3d \rightarrow 2p$	$1 \rightarrow 0$	0.56	Ref. 8
1.00	15.00	15.01	XVII	$3d \rightarrow 2p$	$1 \rightarrow 0$	1.89	Ref. 8
		14.77	XVIII	$3d \rightarrow 2p$	$\frac{3}{2} \rightarrow \frac{1}{2}$	0.26	
		14.77	XVIII	$3d \rightarrow 2p$	$\frac{3}{2} \rightarrow \frac{1}{2}$	0.05	
0.14	14.73	14.76	XVIII	$3d \rightarrow 2p$	$\frac{1}{2} \rightarrow \frac{1}{2}$	0.08	a, Ref. 12
0.19	14.69	14.68	XVIII	$3d \rightarrow 2p$	$\frac{1}{2} \rightarrow \frac{1}{2}$	0.74	b, Refs. 9, 10
0.21	14.66						
		14.59	XVIII	$3d \rightarrow 2p$	$\frac{3}{2} \rightarrow \frac{1}{2}$	0.95	b, Ref. 9
0.43	14.57	14.58	XVIII	$3d \rightarrow 2p$	$\frac{3}{2} \rightarrow \frac{5}{2}$	0.14	
		14.56	XVIII	$3d \rightarrow 2p$	$\frac{3}{2} \rightarrow \frac{1}{2}$	1.05	
0.54	14.52	14.55	XVIII	$3d \rightarrow 2p$	$\frac{3}{2} \rightarrow \frac{3}{2}$	0.14	a, Ref. 10
0.16	14.44	14.46	XVIII	$3d \rightarrow 2p$	$\frac{1}{2} \rightarrow \frac{1}{2}$	0.87	b, Ref. 9
0.41	14.41	14.41	XVIII	$3d \rightarrow 2p$	$\frac{3}{2} \rightarrow \frac{1}{2}$	0.21	b, Ref. 1
		14.37	XVIII	$3d \rightarrow 2p$	$\frac{5}{2} \rightarrow \frac{3}{2}$	0.30	
0.65	14.36	14.35	XVIII	$3d \rightarrow 2p$	$\frac{3}{2} \rightarrow \frac{1}{2}$	0.89	a, Ref. 10
		14.32	XVIII	$3d \rightarrow 2p$	$\frac{1}{2} \rightarrow \frac{1}{2}$	0.39	
0.43	14.25	14.25	XVIII	$3d \rightarrow 2p$	$\frac{1}{2} \rightarrow \frac{3}{2}$	0.12	Ref. 10
		14.20	XVIII	$3d \rightarrow 2p$	$\frac{3}{2} \rightarrow \frac{3}{2}$	0.52	Ref. 10
0.84	14.19	14.19	XVIII	$3d \rightarrow 2p$	$\frac{5}{2} \rightarrow \frac{3}{2}$	0.87	b, Ref. 9
		14.18	XVIII	$3d \rightarrow 2p$	$\frac{3}{2} \rightarrow \frac{1}{2}$	0.59	c, Ref. 12
0.34	14.14	14.15	XVIII	$3d \rightarrow 2p$	$\frac{3}{2} \rightarrow \frac{3}{2}$	0.10	b, Ref. 10
0.47	14.11	14.12	XVIII	$3d \rightarrow 2p$	$\frac{1}{2} \rightarrow \frac{3}{2}$	0.17	Ref. 9
		14.07	XIX	$3d \rightarrow 2p$	$2 \rightarrow 1$	0.75	
0.25	14.02	14.05	XVIII	$3d \rightarrow 2p$	$\frac{3}{2} \rightarrow \frac{1}{2}$	0.63	a, b, Ref. 9
		14.04	XIX	$3d \rightarrow 2p$	$3 \rightarrow 2$	0.65	
0.30	13.94	13.93	XIX	$3d \rightarrow 2p$	$2 \rightarrow 1$	0.29	
0.30	13.93	13.92	XIX	$3d \rightarrow 2p$	$1 \rightarrow 1$	0.15	
0.26	13.88	13.86	XVII	$3p \rightarrow 2s$	$1 \rightarrow 0$	0.13	Ref. 8
0.56	13.81	13.81	XVII	$3p \rightarrow 2s$	$1 \rightarrow 0$	0.77	Ref. 8
0.40	13.79	13.78	XIX	$3d \rightarrow 2p$	$3 \rightarrow 2$	0.65	Ref. 7
0.14	13.76	13.75	XIX	$3d \rightarrow 2p$	$2 \rightarrow 2$	0.20	
		13.75	XIX	$3d \rightarrow 2p$	$2 \rightarrow 1$	0.29	
		13.75	XIX	$3d \rightarrow 2p$	$3 \rightarrow 2$	0.27	Ref. 7
0.18	13.73	13.72	XIX	$3d \rightarrow 2p$	$1 \rightarrow 0$	1.04	Ref. 7
0.22	13.70						
0.36	13.69	13.69	XIX	$3d \rightarrow 2p$	$2 \rightarrow 1$	0.72	
0.29	13.66	13.66	XIX	$3d \rightarrow 2p$	$2 \rightarrow 1$	0.10	
		13.66	XIX	$3d \rightarrow 2p$	$1 \rightarrow 1$	0.07	d, Ref. 9
0.26	13.64	13.64	XIX	$3d \rightarrow 2p$	$3 \rightarrow 2$	0.32	
		13.58	XIX	$3d \rightarrow 2p$	$2 \rightarrow 2$	0.08	Ref. 13
0.29	13.57	13.58	XIX	$3d \rightarrow 2p$	$3 \rightarrow 2$	0.04	Ref. 13
0.83	13.51	13.50	XIX	$3d \rightarrow 2p$	$2 \rightarrow 2$	0.25	Ref. 7
0.36	13.45	13.48	XIX	$3d \rightarrow 2p$	$3 \rightarrow 2$	0.60	e, Ref. 13
0.25	13.42	13.42	XVIII	$3p \rightarrow 2s$	$\frac{3}{2} \rightarrow \frac{1}{2}$	0.19	
0.25	13.40	13.41	XVIII	$3p \rightarrow 2s$	$\frac{5}{2} \rightarrow \frac{3}{2}$	0.15	a, d, Ref. 12
0.29	13.36	13.36	XVIII	$3p \rightarrow 2s$	$\frac{3}{2} \rightarrow \frac{3}{2}$	0.12	a
0.29	13.31	13.28	XIX	$3d \rightarrow 2p$	$3 \rightarrow 2$	0.28	b, Ref. 9

TABLE I *(continued)*.

I	λ (Å)	λ_{calc} (Å)	Charge state	$n'l' \rightarrow nl$	$J' \rightarrow J$	f_{calc}	Footnotes
0.13	13.19						f
0.29	13.16						f
0.27	13.13	13.14	XVIII	$3p \rightarrow 2s$	$\frac{1}{2} \rightarrow \frac{3}{2}$	0.06	
0.56	13.08						d, Ref. 12
0.26	13.04	13.03	XVIII	$3p \rightarrow 2s$	$\frac{3}{2} \rightarrow \frac{1}{2}$	0.16	a, d, Ref. 7, e, Ref. 13

[a] Data suggest more than one transition.
[b] Transition has been previously identified but either different or no J values are given.
[c] Previously identified as a transition in Fe^{XVI}.
[d] Previously identified as a transition in Fe^{XX}.
[e] Previously identified as a transition in Fe^{XXI}.
[f] Transitions in Fe^{XX} near this wavelength.

of the plasma would be required for firm identification of these lines.

A. State specification

States with K-shell vacancies have been ignored, as have states with more than two electrons excited outside the L-shell. Thus the states we consider may be described (Ref. 24)—in LS coupling—

$$1s^2\,2s^x 2p^y[^{S_c}L_c]nl[^SL_J]\,; \qquad (1)$$

x, y, S_c, and L_c specify the "core state" and $nl(^SL_J)$ the "outer electron" (which may be $2p$ for ground-state configurations). The complete set of core states we have considered for eight-, nine-, and ten-electron systems is listed in Table III, with

TABLE II. Prominent observed wavelengths and intensities from 13 to 9.5 Å. The intensities are normalized as in Table I.

I	λ (Å)	Footnotes	I	λ (Å)	Footnotes	I	λ (Å)	Footnotes
0.26	12.97	a, b, Ref. 9	0.17	12.40	d, Ref. 7	0.27	11.31	e, Ref. 13
0.22	12.93	b, Ref. 9	0.24	12.38		0.19	11.24	c, Ref. 12
0.29	12.91		0.17	12.32	a, d, Ref. 13	0.14	11.12	c, Ref. 8
0.29	12.88	b, Ref. 7	0.14	12.28		0.15	11.01	f
0.25	12.84	a, b, Ref. 9	0.28	12.25	c, Ref. 8	0.09	10.92	
0.29	12.81	a, b, Ref. 7	0.13	12.23		0.22	10.80	g, Ref. 24
0.22	12.76		0.18	12.19	a	0.12	10.76	c, Ref. 13
						0.07	10.67	
0.17	12.70		0.30	12.12	c, Ref. 8	0.11	10.65	c, Ref. 13
0.12	12.67	a	0.14	12.07	a	0.09	10.62	a
0.20	12.57	a	0.16	12.03		0.09	10.56	a
0.11	12.54		0.16	11.99		0.09	10.43	
0.20	12.52	c, Ref. 13	0.14	11.96	a	0.15	10.35	a
						0.07	10.17	
0.25	12.49	a	0.28	11.52	e, Ref. 12	0.09	10.14	
						0.07	10.05	
0.20	12.45	a	0.25	11.43	e, Ref. 13	0.12	10.03	
						0.10	9.98	a
0.17	12.42		0.14	11.41		0.10	9.83	d, Ref. 24

[a] Data suggest more than one transition.
[b] Previously identified as a transition in Fe^{XX}.
[c] Previously identified as a transition in Fe^{XVII}.
[d] Previously identified as a transition in Fe^{XXI}
[e] Previously identified as a transition in Fe^{XVIII}.
[f] Our calculations show $4p \rightarrow 2s$, $J_i = 1 \rightarrow J_f = 0$ transition in Fe^{XVII} at 11.01 Å.
[g] Previously identified as a transition in Fe^{XIX}

an identifying index γ and the total number of LS energy levels we have evaluated upon varying n (≤ 5), l (≤ 2), S, and L.

B. Energy levels (in LS coupling)

For the 678 states described in Table III nonrelativistic energies were evaluated using a Hartree-Fock computer code[17] modified to accelerate convergence and automated to facilitate study of such sequences of states as of interest here.

Clementi[26] has discussed relativistic corrections for closed-shell atoms. Similar results may be obtained for open atomic shells. Starting from the Pauli approximation to the Breit equation,[27] the atomic Hamiltonian is written

$$H = H_0 + H_{\rm rel}, \qquad H_{\rm rel} \equiv H_1 + H_2 + H_3 + H_4 + H_5 = O(\alpha^2), \tag{2}$$

where H_0 is the usual nonrelativistic Hamiltonian and

$$H_1 = -\frac{1}{8m^3c^2}\sum_i p_i^4, \tag{3a}$$

$$H_2 = -\frac{1}{4}\frac{e^2}{m^2c^2}\sum_{i\neq j}\frac{1}{r_{ij}}\left(\vec{p}_i\cdot\vec{p}_j + \frac{\vec{r}_{ij}\cdot(\vec{r}_{ij}\cdot\vec{p}_i)\vec{p}_j}{r_{ij}^2}\right), \tag{3b}$$

TABLE III. Core specification of eight-, nine-, and ten-electron systems and the number of LS states evaluated for each.

Eight-electron systems (O sequence)			
$\gamma=1$	$1s^2 2s^2 2p^3(^4S)nl(^2L_J)$		(24 states)
2		(^2D)	(72 states)
3		(^2P)	(56 states)
4	$1s^2 2s2p^4$	$(^4P)nl(^2L_J)$	(56 states)
5		(^2D)	(72 states)
6		(^2S)	(24 states)
7		(^2P)	(56 states)
8	$1s^2 2p^5$	$(^2P)nl(^2L_J)$	(56 states)
Nine-electron systems (F sequence)			
$\gamma=1$	$1s^2 2s^2 2p^4(^3P)nl(^2L_J)$		(56 states)
2		(^1D)	(36 states)
3		(^1S)	(12 states)
4	$1s^2 2s2p^5$	$(^3P)nl(^2L_J)$	(56 states)
5		(^1P)	(28 states)
6	$1s^2 2p^6$	$(^1S)nl(^2L_J)$	(12 states)
Ten-electron systems (Ne sequence)			
$\gamma=1$	$1s^2 2s^2 2p^5(^2P)nl(^2L_J)$		(56 states)
2	$1s^2 2s2p^6$	$(^2S)nl(^2L_J)$	(6 states)

$$H_3 = \frac{\mu}{mc}\left[\sum_i\left(\vec{\xi}_i\times\vec{p}_i + 2e\sum_{j\neq i}\frac{-1}{r_{ij}^3}(\vec{r}_{ij}\times\vec{p}_j)\right)\cdot\vec{S}_i\right], \tag{3c}$$

$$H_4 = \frac{ie\hbar}{(2mc)^2}\sum_i \vec{p}_i\cdot\vec{\xi}_i, \tag{3d}$$

$$H_5 = -\frac{16\pi}{3}\mu^2\sum_{i\neq j}\left[\vec{S}_i\cdot\vec{S}_j\delta(\vec{r}_{ij}) + \frac{1}{r_{ij}^3}\times\left(\vec{S}_i\cdot\vec{S}_j - \frac{3(\vec{S}_i\cdot\vec{r}_{ij})(\vec{S}_j\circ\vec{r}_{ij})}{r_{ij}^2}\right)\right], \tag{3e}$$

α is the fine-structure constant, $\mu = e\hbar/2mc$, and

$$\vec{\xi}_i = Z\frac{\vec{r}_i}{r_i^3} - \sum_{j\neq i}\frac{\vec{r}_{ij}}{r_{ij}^3}$$

determines the electric field at the ith electron. (The summations are taken over the N electrons of the system.)

For Hartree-Fock orbitals standard methods result in the following corresponding relativistic energy corrections:

(i) $$E_1 = -\frac{\alpha^2}{8}\sum_\nu q_\nu[I_1(\nu) - 2l(l+1)I_3(\nu) + l^2(l+1)^2 I_4(\nu)],$$

where q_ν is the occupancy of the νth orbital (ν designating the n, l quantum numbers) and

$$I_1(nl) \equiv \int_0^\infty dr\,[P_{nl}''(r)]^2,$$

$$I_3(nl) \equiv \int_0^\infty dr\,\frac{1}{r^2}P_{nl}''P_{nl}, \quad l>0,$$

$$I_4(nl) \equiv \int_0^\infty dr\,\frac{1}{r^4}P_{nl}^2, \quad l>0.$$

In obtaining these expressions, the Hartree-Fock orbitals are written

$$\langle\vec{r}\,|nlm\rangle = (1/r)P_{nl}(r)Y_{lm}(\hat{r}).$$

(ii) $E_2 \equiv 0$ for a product wave function.[27]

(iii) H_3 contains the spin-orbit interactions, and may be rewritten[28]

$$H_3 = \zeta_c{\sum_i}'\vec{l}_i\cdot\vec{S}_i - \frac{\alpha^2}{2}{\sum_{i\neq j}}'\left(\frac{\vec{r}_{ij}}{r_{ij}^3}\times\vec{p}_i\right)\cdot(\vec{S}_i + 2\vec{S}_j) = H_{\rm SO} - H_3',$$

where the prime indicates that the summation is restricted to open shells only. Evaluation of the spin-orbit energy $E_{\rm SO}$ is described in Sec. IC below. The spin–other-orbit energy E_3' may be evaluated using Ref. 28 [Eqs. (13) and (18)], and is generally dominated by the same-shell terms, for which Horie[29] has given expressions in terms

TABLE IV. Total relativistic energy of some eight-electron systems on an iron nucleus and its elements.

Configuration	E_1 (eV)	E_4+E_5 (eV)	ϵ_{rel} (eV)
$1s^2 2s^2 sp^4(^3P)$	$E_{HF}=-28,397$ eV		
$(1s)^2$	−794.0	+642.0	−152.0
$(2s)^2$	−100.0	63.7	− 36.3
$(2p)^4$	− 30.5	0.08	− 30.5
			$E_{rel}=-219.0$
$1s^2 2s2p^5(^3P)$	$E_{HF}=-28,295$ eV		
$(1s)^2$	−793.0	642.0	−151.0
$2s$	− 50.6	32.1	− 18.5
$(2p)^5$	− 37.8	0.10	− 37.7
			$E_{rel}=-207.0$
$1s^2 2p^6(^1S)$	$E_{HF}=-28,162$ eV		
$(1s)^2$	−793.0	642.0	−151.0
$(2p)^6$	− 45.2	0.12	− 45.0
			$E_{rel}=-196.0$

of orbital integrals provided by the Froese code.[17] In our results here we find this residual spin-other-orbit energy to be unimportant and have accordingly neglected it.

(iv) $$E_4=\frac{\alpha^2}{8}\left(\sum_\nu q_\nu I_5(\nu)-\sum_\nu q_\nu(q_\nu-1)I_2(\nu)-\sum_{\nu\neq\nu'} q_\nu q'_\nu I_{22}(\nu,\nu')\right),$$

in terms of

$$I_5(nl)\equiv Z[(1/r)P^2_{n,l=0}]_{r=0},\quad l=0 \text{ only},$$

$$I_2(nl)\equiv\int_0^\infty \frac{dr}{r^2}P^4_{nl},$$

$$I_{22}(nl,n'l')\equiv\int_0^\infty dr\frac{1}{r^2}P^2_{nl}P^2_{n'l'}.$$

(v) H_5 contains two contributions, $H_5=H_{51}+H_{52}$. E_{51} is the spin-contact term,

$$E_{51}=\frac{\alpha^2}{8}\left(\sum_\nu (q_\nu^2-\delta_{q_\nu,1})I_2(\nu)+\sum_{\nu\neq\nu} q_\nu q_{\nu'} I_{22}(\nu,\nu')\right),$$

and is generally combined directly with E_4. E_{52} is the spin-dipole-dipole term and is nonvanishing only between pairs of open shells. The same-shell terms dominate, may be evaluated similarly to H'_3 above, and are similarly small. In our results here the term E_{52} has been ignored.

Thus we approximate the total relativistic energy by

$$E_{tot}=E_{HF}+E_{rel}=E_{HF}+(E_1+E_4+E_{51}), \quad (4)$$

E_{HF} being the nonrelativistic Hartree-Fock energy. In Table IV we present the various elements of Eq. (4), broken down by orbital, for a few eight-electron states. As we see, the relativistic energy per orbital is relatively insensitive to occupancy and coupling, and the total is additive. The orbital energies do vary slowly with the total number of bound electrons. In Table V we list approximate orbital energies per electron, $\epsilon_\nu(N)$, for five through ten electrons bound to an iron nucleus such that the total relativistic correction may be written in terms of the orbital occupation q_ν as

$$E_{rel}=\sum_\nu q_\nu\epsilon_\nu$$

to within a few percent accuracy.

C. Intermediate coupling

As is well known,[30] intermediate-coupling calculations are necessary for state identification of ten-electron systems, even for the neutral species Ne. With increasing nuclear charge, LS coupling is expected to become less and less appli-

TABLE V. Number of allowed transitions.

N (electrons)	LS coupling	Intermediate coupling	
5	603		
6	1021		
7	1068		
8	661		1366
9	167		281
10	9		21

cable. Accordingly we have transformed our numerical *LS* Hartree-Fock results to an intermediate coupling representation. Two energy contributions which are nondiagonal in *LS* coupling have been considered.

(i) The spin-orbit terms result from the nondiagonal matrix elements of H_{SO} [Eq. (3c) above]. The numerical Hartree-Fock code evaluates the usual spin-orbit parameters ζ_{2p} and ζ_{nl} from the computed radial orbitals.[31] Standard Racah algebra techniques[32] allow expression of H_{SO} matrix elements in terms of these. We simply present our results. In general,

$$E_3 = \left\langle \cdots ({}^S L_J) \left| \sum_i \xi_i \vec{l}_i \cdot \vec{s}_i \right| \cdots ({}^{S'} L'_J) \right\rangle$$

$$= (-1)^{S'+L+J} \begin{Bmatrix} J & S & L \\ 1 & L' & S' \end{Bmatrix} \times [(2L+1)(2L'+1)(2S+1)(2S'+L)]^{1/2} \xi_3 . \quad (5)$$

Two open shells. (a) For

$$\langle p^n ({}^{S_c} L_c) l ({}^S L_J) | \cdots | p^n ({}^{S'_c} L'_c) l ({}^{S'} L'_J) \rangle ,$$

the following equation holds:

$$\xi_3 = \xi_{31} + \xi_{32},$$

where

$$\xi_{31} = \zeta_{2p} (-1)^{L_c+l+L'} \begin{Bmatrix} L_c & L & l \\ L' & L'_c & 1 \end{Bmatrix} (-1)^{S_c+1/2+S'} \times \begin{Bmatrix} S_c & S & \frac{1}{2} \\ S' & S'_c & 1 \end{Bmatrix} \Gamma ({}^{S_c} L_c | p^n | {}^{S'_c} L'_c) , \quad (5a)$$

$\Gamma(\cdots | p^n | \cdots) = (\cdots | \sqrt{6} V''(p^n) | \cdots)$ is tabulated by Racah (Tables X and XI of Ref. 33), and

$$\xi_{32} = \zeta_{nl} (-1)^{L'_c+l+L} \begin{Bmatrix} l & L & L_c \\ L' & l & 1 \end{Bmatrix} (-1)^{S'_c+1/2+S} \times \begin{Bmatrix} \frac{1}{2} & S & S_c \\ S' & \frac{1}{2} & 1 \end{Bmatrix} 3 \delta_{L_c L'_c} \delta_{S_c S'_c} ; \quad (5b)$$

(b) for

$$\langle s[p^n ({}^{S_P} L_P)] ({}^S L_J) | \cdots | s[p^n ({}^{S'_P} L'_P)] ({}^{S'} L'_J) \rangle ,$$

the following equation holds:

$$\xi_3 = \zeta_{2p} \frac{\delta_{LL_p} \delta_{L' L'_p}}{[(2L+1)(2L'+1)]^{1/2}} (-1)^{S'_p+1/2+S} \times \begin{Bmatrix} S_p & S & \frac{1}{2} \\ S' & S'_p & 1 \end{Bmatrix} \Gamma ({}^{S_P} L_p | p^n | {}^{S'_P} L'_P) \quad (5c)$$

Three open shells. For the form

$$\langle s[p^n ({}^{S_P} L_c)] ({}^{S_c} L_c) l ({}^S L_J) | \cdots | s[p^n ({}^{S'_P} L'_c)] ({}^{S'_c} L'_c) l ({}^{S'} L'_J) \rangle ,$$

the following equation holds:

$$\xi_3 = \xi'_{31} + \xi_{32} ,$$

where

$$\xi'_{31} = (-1)^{S'_p+S_c+3/2} [(2S_c+1)(2S'_c+1)]^{1/2} \times \begin{Bmatrix} S_P & S_c & \frac{1}{2} \\ S'_c & S'_P & 1 \end{Bmatrix} \xi_{31}, \quad (5d)$$

and ξ_{31} and ξ_{32} are from Eqs. (5a) and (5b) above.

(ii) Nondiagonal electric terms have been described by Slater,[31] who tabulates expressions for the regular coefficients. The necessary radial integrals have been evaluated by averaging our numerical Hartree-Fock results over the contributing *LS* values. The variation of the individual values about their average is generally less than a few percent of their value, owing to the small coupling dependence of the radial orbitals.

Given the energy matrix elements which are nondiagonal in *LS* coupling, the energy matrix was diagonalized numerically. Table VI contains some examples of the results for eight-, nine-, and ten-electron systems bound to an iron nucleus ($Z = 26$). The total Hartree-Fock binding energy W_{HF} of the system and the relativistic correction W_{rel} are presented, as well as the successively more detailed excitation energies E (eV): (i) $E({}^S L)$, Hartree-Fock excitation energy (with relativistic corrections); (ii) $E({}^S L_J)$, the above with J splitting treated by first-order perturbation theory; (iii) $E_J^{(1)}$, the corresponding energy resulting from the intermediate-coupling calculation with only the nondiagonal, spin-orbit interaction included; and (iv) $E_J^{(2)}$, the full intermediate-coupling energy, including both electric and spin-orbit, nondiagonal interactions.

It is apparent that the relativistic and intermediate-coupling energy shifts are of comparable magnitude. As seen from comparison with data (Tables I and II), a discrepancy between theory and experiment of less than 0.25% is observed, so the necessity of calculating such detailed effects is apparent. For each ionization state, we have included in Table VI examples of configurations between which radiative transitions are observed, and have indicated with an asterisk the excitation energies corresponding to *L-S* forbidden transitions. The observed spectrum is much richer than would be predicted by *LS* coupling. Thus the dominating reason for an intermediate-coupling calculation is for spectral identification.

TABLE VI. Some examples of the change in calculated spectrum when intermediate coupling is included. (Excitation energies corresponding to L-S forbidden transitions are indicated by an asterisk.)

State	S	L	J	Total energy (eV) W_{HF}	W_{rel}	Excitation energy $E(^SL)$	$E(^SL_J)$	Intermediate coupling $E_J^{(1)}$	$E_J^{(2)}$
Ne: $2p^6(^1S)$	0	0	0	−31 012	−226.8	0	0	0	0
$2p^5(^2P)3d$	0	1	1	−30193	−223.3	822.5	823.1	826.0	826.0*
	1	1	1	−30 204	−223.2	811.5	813.8	812.1	812.1*
$2s2p^6(^2S)3p$	0	1	1	−30128	−213.5	897.3	897.6	898.1	898.1
	1	1	1	−30131	−213.6	894.2	895.0	894.5	894.5*
F: $2p^5(^2P)$	$\frac{1}{2}$	1	$\frac{1}{2}$	−29751	−223.1	0	12.4	12.4	12.4
	$\frac{1}{2}$	1	$\frac{3}{2}$	−29751	−223.1	0	0	0	0
$2p^4(^1D)3d$	$\frac{1}{2}$	0	$\frac{1}{2}$	−28891	−219.1	864.0	867.7	870.1	869.8
	$\frac{1}{2}$	1	$\frac{1}{2}$	−28891	−219.0	864.1	868.5	871.8	878.2
	$\frac{1}{2}$	1	$\frac{3}{2}$	−28891	−219.0	864.1	868.3	870.5	873.0
	$\frac{1}{2}$	2	$\frac{3}{2}$	−28890	−219.0	865.1	869.2	871.8	876.2
	$\frac{1}{2}$	2	$\frac{5}{2}$	−28890	−219.0	865.1	869.6	871.9	873.8
	$\frac{1}{2}$	3	$\frac{5}{2}$	−28890	−219.0	865.1	868.4	870.7	869.7*
O: $2s^22p^4(^3P_J)$	1	1	0	−28397	−218.9	0	13.6	9.72	9.72
	1	1	1	−28397	−218.9	0	8.66	10.6	10.6
	1	1	2	−28397	−218.9	0	0	0	0
$2s2p^4(^2D)3p(^SL_J)$	0	1	1	−27424	−204.5	987.5	991.6	994.8	994.3*
	0	2	2	−27425	−204.5	986.4	990.7	994.0	991.5*
	0	3	3	−27429	−204.5	982.4	986.9	988.6	988.3*
$2s^2p^4(^2D)3p(^SL_J)$	1	1	0	−27427	−204.4	984.5	989.8	990.8	990.9
	1	1	1	−27427	−204.4	984.5	989.3	990.1	993.2
	1	1	2	−27427	−204.4	984.5	988.3	990.5	996.3
	1	2	1	−27428	−204.5	983.4	987.4	987.7	987.8
	1	2	2	−27428	−204.5	983.4	987.8	989.3	989.1
	1	2	3	−27428	−204.5	983.4	988.3	991.7	991.6
	1	3	2	−27432	−204.5	979.4	982.7	983.7	984.0*
	1	3	3	−27432	−204.5	979.4	983.8	985.6	985.9*

D. Transition probabilities

Given the energy levels, wave functions, and intermediate-coupling amplitudes, application of the familiar electric dipole selection rules determines the spectrum. The intermediate-coupling amplitudes are the coefficients C_{LS}^J of the expansion

$$\psi_J = \sum_{LS} C_{LS}^J \psi_{LS},$$

where ψ_J is the intermediate-coupling wave function and the ψ_{LS} are its constituent LS wave functions evaluated by our numerical Hartree-Fock equation.

The numbers of lines obtained (with energy $\hbar\omega > 700$ eV) in strictly LS coupling and in intermediate coupling are given in Table VII.

For each allowed transition found by this process an f number is evaluated, according to[24]

$$g_i f_{ij} = \tfrac{1}{3}(\hbar\omega_{ij}/\mathcal{R}_\infty) S(J) \sigma_{ij}^2 ; \qquad (6)$$

g_i is the statistical factor, $\hbar\omega_{ij}$ is the transition energy, $\mathcal{R}_\infty \simeq 13.6$ eV is the Rydberg constant, $S(J)$ is the result of the angle integrations, expressed as the square of the sum over LS terms weighted by C_{LS}^J, or more succinctly by Cowan,[34] and σ_{ij}^2 is the radial matrix element. In the results presented here the radial integral has been evaluated by the Coulomb approximation[21] and not by integrating the Hartree-Fock wave functions, so our f-number values are accordingly less accurate but are sufficient for our purposes here.

TABLE VII. Relativistic orbital energy corrections (eV) for N electrons on an iron nucleus.

	$N=5$	6	7	8	9	10
$1s$	−76.7	−76.6	−76.5	−76.4	−75.9	−75.4
$2s$	−20.8	−20.1	−19.3	−18.5	−18.0	−17.6
$2p$	− 8.8	− 8.6	− 8.1	− 7.5	− 7.3	− 7.2
$3s$	− 6.6	− 6.0	− 5.8	− 5.5	− 5.0	− 4.5
$3p$	− 3.4	− 3.1	− 2.8	− 2.6	− 2.3	− 2.0
$3d$	− 1.1	− 0.98	− 0.85	− 0.73	− 0.62	− 0.51

IV. SUMMARY

The x-ray spectrum of a laser-produced Fe plasma has been observed with a curved-crystal spectrograph between the wavelengths 9.5 and 17.0 Å. Wavelengths and relative intensities have been determined for 96 lines.

For the strongest part of the spectrum, above 13 Å, almost all of the observed lines have been identified as radiation from Fe^{XVII}, Fe^{XVIII}, and Fe^{XIX} ions. Full intermediate-coupling, Hartree-Fock calculations with relativistic corrections give calculated wavelengths which agree with the experiment to within less than 0.25%. Because of the strong intermediate coupling, transitions are identified by the total angular momentum of the initial and final states and by the single electron transition.

ACKNOWLEDGMENTS

The authors (L.F.C. and W.C.J.) are indebted to Dr. Dungee and his staff at Battelle Memorial Institute, especially Dr. Mallozzi, Dr. Applebaum, Dr. Epstein and W. J. Gallagher, for their kindness and cooperation in making these experiments possible. Also, the authors wish to gratefully acknowledge the help of T. D. Miller of Lockheed for his assistance in the experimental portion of the program.

---

*Work supported in part by the Lockheed Independent Research Program and the Defense Nuclear Agency.

[1]B. C. Fawcett, A. H. Gabriel, and P. A. H. Saunders, Proc. Phys. Soc. Lond. 90, 863 (1967).
[2]K. Evans and K. A. Pounds, Astrophys. J. 152, 319 (1968).
[3]W. H. Tucker and M. Koren, Astrophys. J. 168, 283 (1971).
[4]B. C. Fawcett, J. Phys. B 4, 981 (1971).
[5]J. H. Parkinson, Astron. Astrophys. 24, 215 (1973).
[6]M. Loulergue and H. Nussbaumer, Astron. Astrophys. 24, 209 (1973).
[7]B. C. Fawcett, R. D. Cowan, and R. W. Hayes, Astrophys. J. 187, 377 (1974).
[8]F. Tyren, Z. Phys. 111, 314 (1938).
[9]U. Feldman and L. Cohen, Astrophys. J. 151, L55 (1968).
[10]L. Cohen, U. Feldman, and S. O. Kastner, J. Opt. Soc. Am. 58, 331 (1968).
[11]L. Cohen and U. Feldman, Astrophys. J. 160, L105 (1970).
[12]J. P. Connerade, N. J. Peacock, and R. J. Speer, Solar Phys. 14, 159 (1970).
[13]M. Swartz, S. Kastner, E. Rothe, and W. Neupert, J. Phys. B 4, 1747 (1971).
[14]U. Feldman, G. A. Doschek, R. D. Cowan, and L. Cohen, J. Opt. Soc. Am. 63, 1445 (1973).
[15]P. J. Mallozzi, H. M. Epstein, R. G. Jung, D. C. Applebaum, B. P. Fairand, W. J. Gallagher, R. L. Necker, and M. C. Muckerheide, J. Appl. Phys. 45, 1891 (1974).
[16]L. F. Chase, R. K. Bardin, T. R. Fisher, H. A. Grench, W. C. Jordan, D. A. Kohler, R. K. Landshoff, T. D. Miller, and J. G. Pronko, X-Ray Diagnostics for Laser Systems, Lockheed Palo Alto Research Laboratory Report LMSC-D401229 (1974) (unpublished).
[17]C. Froese, Can. J. Phys. 41, 1895 (1963).
[18]R. Chapman, Astrophys. J. 152, 319 (1968).
[19]H. Rugge and A. B. C. Walker, J. Space Res. 8, 439 (1970).
[20]G. A. Doschek, J. F. Meekins, and R. D. Cowan, Solar Phys. 25, 125 (1973).
[21]D. R. Bates and A. Damgaard, Philos. Trans. R. Soc. A 242, 101 (1949).
[22]M. Loulergue, Astron. Astrophys. 15, 216 (1971).
[23]J. A. Bearden, Rev. Mod. Phys. 39, 78 (1967).
[24]B. H. Armstrong, R. R. Johnston, and R. S. Kelly, in *Progress in High Temperature Physics and Chemistry* (Pergamon, Oxford, 1967), Vol. I.
[25]R. R. Johnston, R. K. M. Landshoff and O. R. Platas, Radiative Properties of High Temperature Air, Lockheed Palo Alto Research Laboratory Report LMSC D267205 (1972) (unpublished).
[26]E. Clementi, Phys. Rev. 133, A1295 (1964).
[27]H. A. Bethe and E. Salpeter, *Quantum Mechanics of One- and Two-Electron Atoms* (Academic, New York, 1957), Eq. (39.14).
[28]M. Blume and R. E. Watson, Proc. R. Soc. A 270, 127 (1962).
[29]H. Horie, Progr. Theor. Phys. (Kyoto) 10, 296 (1953).
[30]C. E. Moore, *Atomic Energy Levels*, Natl. Bur. Stand. Circ. No. 467 (U. S. GPO, Washington D. C., 1949), Vol. I.
[31]J. C. Slater, *Theory of Atomic Structure* (McGraw-Hill, New York, 1960), Vol. II, Appendix 21.
[32]A. R. Edmonds, *Angular Momentum in Quantum Mechanics* (Princeton U. P., Princeton, N. J., 1960).
[33]G. Racah, Phys. Rev. 63, 367 (1943).
[34]R. D. Cowan, J. Opt. Soc. Am. 58, 808 (1968).